Real-Time Emulation of Grid-Connected DFIG Wind Energy System with Model Validation from Sub-synchronous to Hyper-synchronous Operation under Unbalanced Conditions

Maximiliano Ferrari*, Emilio C. Piesciorovsky** , Leon M. Tolbert†

* Grid Components and Control, Oak Ridge National Laboratory, Oak Ridge, TN, USA, 37830

** Power Systems Resiliency, Oak Ridge National Laboratory, Oak Ridge, TN, USA, 37830

† The University of Tennessee, Knoxville, TN, USA, 37996

2022 IEEE Power & Energy Society General Meeting (PESGM) | 978-1-6654-0823-3/22/$31.00 ©2022 IEEE | DOI: 10.1109/PESGM48719.2022.9916807

***Abstract*—Previous work on real-time simulation of DFIGs have assumed that the generator model is valid over a wide range of operating speeds and for multiple grid voltage unbalances. However, this assumption has not been tested in the literature, which limits the accuracy of results obtained in both simulations and in hardware-in-the-loop (HIL) applications. To address this gap in the literature, this paper presents a preliminary model validation of the DFIG with iron losses and demonstrates the limitations of the model in accurately representing a physical DFIG machine under grid unbalanced operation. This paper implements all the required discrete models for real-time emulation of the DFIG on a field programmable gate array (FPGA), including: the dynamic model of the DFIG, rotor side converter (RSC), grid side converter (GSC), and aerodynamic and mechanical models. Also included are key implementation aspects of the hardware-testbed utilized for the model validation, which consists of a DFIG machine connected to a partial-scaled four-quadrant back-to-back power converter. The DFIG machine models utilized for this research are available to the public and can be accessed in a GitHub repository listed in the references.**

***Index Terms*-- wind energy testbed, type-3 wind turbine, doubly-fed induction generator, real-time simulation**

I. Introduction

Doubly-fed induction generators (DFIGs) have been broadly used in variable speed wind energy conversion systems due to their competitive cost, durability, flexible power control, and variable speed capacity using a partial-scaled converter [1]. These advantages have made the DFIG one of the leading technologies in the wind turbine sector as well as the most installed variable speed wind turbine in the United States [1-3]. Due to the DFIG's preeminence as a renewable energy technology, combined with grid codes requiring increased capability during voltage and frequency grid events [4-6], it is becoming increasingly important for the research community and the industry to have a better understanding of the grid-connected DFIG systems' operations during various grid conditions. However, applied research on a full-scale utility system is limited due to prohibitive costs and safety concerns. Laboratory testbeds are an alternative to study full-scale systems [7-9]. These designs offer a reliable representation of the DFIG system; however, this approach also presents inhibiting factors including high cost, high complexity, long development times, and steep associated learning curve. Commercial real-time simulators, including RTDS, OPAL-RT, StarSim, Plexim, and Typhoon, remove many technical barriers and reduce development times but can still be prohibitively expensive [10-12]. Although these simulators are a powerful auxiliary platform to hardware implementation that allow study and simulation of a system in real-time, they require proprietary hardware and licensing, and the validity of the models is typically not published.

In the face of these many challenges of studying systems in real-time, one economically accessible and technically proficient option is to implement the discrete models directly on Digital Signal Processors (DSPs) or Field Programmable Gate Arrays (FPGA). This approach removes some of the barriers while permitting the access of intermediary variables that are not typically available in pre-built, commercial models. Some authors have taken this approach to emulate real-time wind energy systems. For example, researchers in [14] implemented the electrical and mechanical discrete models of the DFIG and the permanent-magnet synchronous generator (PMSG) on a real-time computer Nexcom NISE 3140. Authors in [13] developed a real-time simulation DFIG wind turbine to evaluate interconnection challenges, where a 7-bus grid was simulated in RTDS and the wind system is deployed on a DSP cluster. In [15], the authors compiled into C-code a complete DFIG system and executed it on a PC-cluster real-time simulator. Although these papers address the discrete-modeling and implementation for real-time applications, critically, they lack details regarding the validity of the implemented models, which can limit the reliability of the obtained results.

Although extensive research has been done regarding real-time modeling and simulation. The published papers in real-time simulations typically do not provide details about the validity of the models. If the models used in real-time simulations are not accurate representations of the real system, their utility as a replacement for research purposes is severely limited. Focusing on DFIGs [16-18], only a few papers address the model validation against physical hardware. For example,

ACKNOWLEDGEMENT Research sponsored by the Laboratory Directed Research and Development Program of Oak Ridge National Laboratory, P.O. Box 2008, Oak Ridge, Tennessee 37831-6285; managed by UT Battelle, LLC, for the U.S. Department of Energy. This manuscript has been authored by UT-Battelle, LLC, under contract DE-AC05- 00OR22725 for the U.S. Department of Energy. The United States Government retains and the publisher, by accepting the article for publication, acknowledges that the United States Government retains non-exclusive, paid-up, irrevocable, worldwide license to publish or reproduce the published form of this manuscript, or allow others to do so, for United States Government purposes.

978-1-6654-0823-3/22/$31.00 ©2022 IEEE

authors in [16] present a comparison of the DFIG model for three-phase voltage dips and unbalanced voltage sags for a 3 MW DFIG. Authors in [17] present a DFIG model validation of a laboratory-scale DFIG for voltage sags. Although some of these studies do use field data to validate the DFIG machine, the validation is limited to power quality issues. The full-range validation of the DFIG has been overlooked in the literature. As a preliminary step in addressing this gap in knowledge, this study presents a validation of the DFIG model against a scaled-down DFIG. The model selected for this study is the αβ model oriented with the rotor angles, which is a classical model used to study DFIG operation. The iron losses were included in the model used for the validation because low-power machines like the one used for this study are lossy in comparison with full-rated machines. The DFIG machine models utilized for this research as well as the experimental results available to the public and can be accessed in a GitHub repository listed in the reference [24].

The structure of this paper is as follows: Section I develops the real-time models of the DFIG dynamic model, back-to-back inverter model, mechanical model, and aerodynamic model. This section provides a benchmark that compares the classical DFIG models in terms of FPGA resources utilization. Section II describes the hardware prototype testbed and control of the power converter. Section III presents the model verification against a physical DFIG setup. Finally, Section IV presents the conclusions.

II. Real-time discrete models

A. Real-Time Emulation of DFIG

The DFIG dynamic model describes the behavior of the machine in steady state as well the evolution of the electric variables during transients [1]. The review of literature shows four different reference frames that are used to express the electrical variables of the DFIG: the αβγ oriented with the stator or rotor angles, synchronous (dqo), and natural frame dynamic models [19,22]. These models can be represented in matrix form using currents or fluxes as state variables. Fig. 1 shows a benchmark between these models in terms of execution time and FPGA slices utilization. For this comparison, the compilation results of four independent compilations were averaged, and neither the compiler nor the code were optimized in any way.

Fig. 1 shows that the chosen reference frame and the state-variable representation impact the model execution time and FPGA logic requirements. Although the DFIG αβ model that uses the fluxes as state variables is proven to be efficient for real-time applications, it does not take into consideration the core loss, which is considerable in low power machines such as the one utilized in this study. Neglecting the iron losses in low power machines introduces substantial errors in the estimation of the rotor and stator currents. To provide a model as close as possible to the real machine, the iron loss is introduced in the model. As shown in Fig. 1, introducing the iron losses increases the loop time execution to 60 µs and requires 15% of the logic resources in the Xilinx Kintex-7 7K325T FPGA. For MW machines, the iron losses can be neglected, and a more efficient model can be used instead. Fig. 2 shows the computer implementation of a DFIG dynamic model that include iron losses and the one used in this study [21].

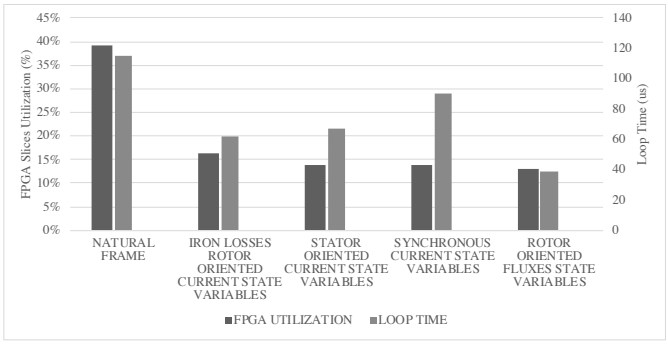

Fig. 1. FPGA utilization and loop time for different DFIG machine models.

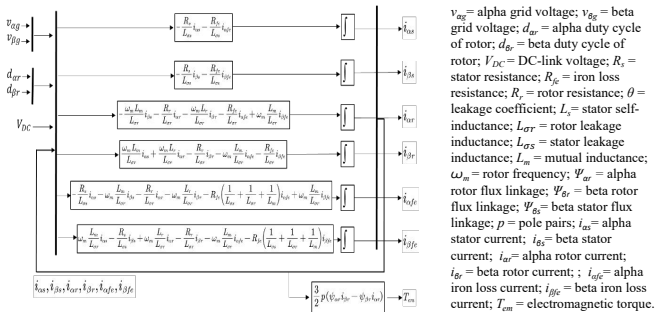

$v_{\alpha g}$= alpha grid voltage; $v_{\beta g}$ = beta grid voltage; $d_{\alpha r}$ = alpha duty cycle of rotor; $d_{\beta r}$ = beta duty cycle of rotor; V_{DC}= DC-link voltage; R_s = stator resistance; R_{fe} = iron loss resistance; R_r = rotor resistance; θ = leakage coefficient; L_s= stator self-inductance; $L_{\sigma r}$ = rotor leakage inductance; $L_{\sigma s}$ = stator leakage inductance; L_m = mutual inductance; ω_m = rotor frequency; $\Psi_{\alpha r}$ = alpha rotor flux linkage; $\Psi_{\beta r}$ = beta rotor flux linkage; $\Psi_{\beta s}$= beta stator flux linkage; p = pole pairs; $i_{\alpha s}$= alpha stator current; $i_{\beta s}$= beta stator current; $i_{\alpha r}$= alpha rotor current; $i_{\beta r}$ = beta rotor current; ; $i_{\alpha fe}$= alpha iron loss current; $i_{\beta fe}$ = beta iron loss current; T_{em} = electromagnetic torque.

Fig. 2. Computer implementation of the DFIG considering iron loss [21].

B. Power Converter Model

Different types of converter topologies have been proposed for wind applications; however, the most common choice for the DFIG is the back-to-back converter [8]. The back-to-back model consists of a grid-side converter (GSC) and rotor-side converter (RSC.)

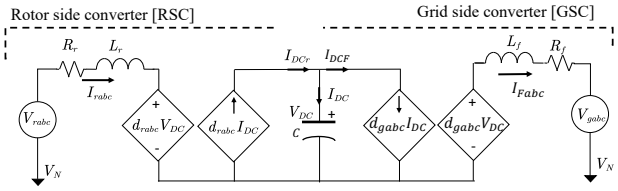

V_N = neutral voltage; V_{rabc} = a, b, c phase rotor voltages; R_r = rotor resistance; L_r = rotor self-inductance; I_{rabc} = a, b, c phase rotor currents; d_{rabc}= a, b, c phase duty cycles of rotor controller side; V_{DC}= DC-link voltage; I_{DC} = DC-link current; I_{DCr} = DC-link current of rotor; I_{DCF} = DC-link current of grid filter; C = circuit capacitance; d_{Fabc} = a, b, c phase duty cycle of grid controller side; I_{Fabc} = a, b, c phase grid filter currents; L_f = grid filter inductance; R_f = grid filter resistance; V_{gabc} = a, b, c phase grid voltages

Fig. 3. Average model for a back-to-back converter.

Fig. 3 shows an average model for a back-to-back converter. Applying Kirchhoff's law on the circuit of Fig. 3 and choosing currents as state-variables, the average model of the GSC is represented by (1), the RSC by (2), and the DC-link circuit by (3):

$$\frac{d}{dt}\vec{i}_{Fabc} = \frac{R_f}{L_f}\,\vec{i}_{Fabc} + \frac{1}{L_f}\,\vec{v}_{abc} - \frac{1}{L_f}\,\vec{v}_n - \frac{V_{DC}}{L_f}\,\vec{d}_{Fabc} \quad (1)$$

$$\frac{d}{dt}\vec{\imath}_{rabc} = \frac{R_r}{L_r}\,\vec{\imath}_{rabc} + \frac{R_r}{L_r}\,\vec{v}_{rabc} + \frac{1}{L_r}\,\vec{v}_n - \frac{V_{DC}}{L_r}\,\vec{d}_{rabc} \tag{2}$$

$$\frac{d}{dt}V_{DC} = \frac{1}{C}\left(\left[\overrightarrow{dT}_{rabc}\right]\vec{\imath}_{rabc} - \overrightarrow{dT}_{Fabc}\;\vec{d}_{Fabc}\right) \tag{3}$$

Where, $\vec{\imath}_{Fabc} = \begin{bmatrix} i_{Fa} \\ i_{Fb} \\ i_{Fc} \end{bmatrix}$, $\vec{v}_{abc} = \begin{bmatrix} v_a \\ v_b \\ v_c \end{bmatrix}$, $\vec{v}_n = \begin{bmatrix} v_n \\ v_n \\ v_n \end{bmatrix}$, $\vec{d}_{Fabc} = \begin{bmatrix} d_{Fa} \\ d_{Fb} \\ d_{Fc} \end{bmatrix}$, $\vec{\imath}_{rabc} = \begin{bmatrix} i_{ra} \\ i_{rb} \\ i_{rc} \end{bmatrix}$, $\vec{v}_{rabc} = \begin{bmatrix} v_{ra} \\ v_{rb} \\ v_{cr} \end{bmatrix}$, $\vec{d}_{rabc} = \begin{bmatrix} d_{ra} \\ d_{rb} \\ d_{rc} \end{bmatrix}$.

C. Mechanical Model

Previously developed mechanical models include complex models of six masses or three masses [8]. However, the two-mass model is the simplest and provides reasonable accuracy. Assuming a perfect rigid low speed shaft, the two-mass drivetrain model is reduced to a one-mass drivetrain model. The governing equation [1] is represented by (4):

$$\frac{d}{dt}\omega = \frac{P}{J}\,(T_{WT} - T_{EM}) \tag{4}$$

where ω is rotor speed in rad/s, p is the pole pairs, J is the inertia, T_{WT} is mechanical torque of wind turbine, and T_{EM} is the electromagnetic torque.

D. Aerodynamic Model

The mechanical output power that could be extracted from a three-blade wind turbine is given by,

$$P_{WT} = \frac{1}{2}\,\rho\,\pi\,R_{WT}^2\,C_p(\beta,\lambda)\,v_{wind}^3 \tag{5}$$

where P_{WT} is the mechanical output power of the turbine in [W], ρ is the air density in [kg/m^3], R_{WT} is the blade length of wind turbine in [m], C_p is the performance coefficient of the wind turbine, β is the blade pitch angle in degrees, λ is the tip speed ratio of the wind turbine blade, v_{wind} is the wind speed in [m/s]. The performance coefficient of the turbine (C_p) can be approximated by,

$$C_p(\beta,\lambda) = 0.5176\left(\frac{116}{\lambda_i} - 0.4\beta - 5\right)e^{\frac{-21}{\lambda_i}} + \frac{6.8\lambda}{1000} \tag{6}$$

$$\lambda = R_{WT}\,\frac{\omega_m}{v_{wind}} \tag{7}$$

$$\frac{1}{\lambda_i} = \frac{1}{\lambda - 0.08\beta} - \frac{0.035}{\beta^3 + 1} \tag{8}$$

where R_{WT} is the blade radius of wind turbine in m.

III. Hardware Testbed

This section describes the hardware testbed used to verify the dynamic behavior of the DFIG model. Fig. 4(a) and (b) show the control and interconnections of the hardware testbed, which consists of a Motor Solver DFIG generator, a Viewpoint back-to-back converter, grid filters, and a permanent magnet

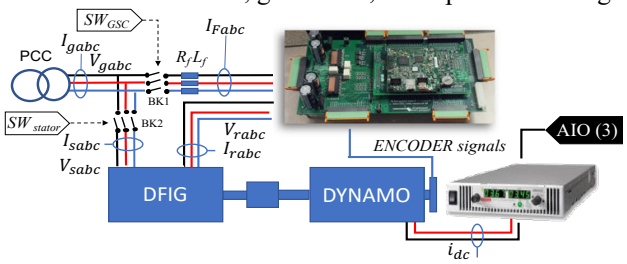

SW_{GSC} = BK1 control signal; Sw_{stator} = BK2 control signal; V_{sabc} = *a, b, c* stator phase stator voltages; V_{gabc} = *a, b, c* grid phase grid voltages; V_{rabc} = *a, b, c* rotor phase voltages; I_{gabc} = *a, b, c* grid phase currents; I_{sabc} = *a, b, c* stator phase currents; i_{rabc} = *a, b, c* rotor phase currents; I_{fabc} = *a, b, c* grid phase converter currents; i_{dc} = DC current of torque-controlled permanent magnet motor; L_f = grid filter inductance; R_f = grid filter resistance; AIO(3) = DC supply current reference; DFIG = Double fed induction generator; DYNAMO = DC Permanent magnet motor.

(a) Electrical schematic of DFIG testbed

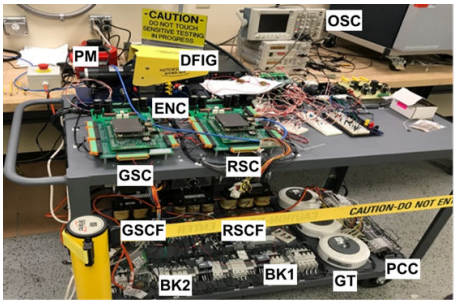

OSC: Oscilloscope
DFIG: Double fed induction generator
PM: Permanent magnet motor
ENC: Encoder
GSC: Grid side converter
RSC: Rotor side converter
PCC: Point of common coupling
BK1: Grid breaker
BK2: Stator breaker
GT: Step up grid transformers
GSCF: Grid side converter filter
RSCF: Rotor side converter filter

(b) DFIG Hardware testbed

Fig. 4. Electric schematic (a) Hardware testbed (b) for DFIG testbed.

(PM) driver used to emulate the wind model. The power converter controller was implemented on a NI-cRIO 9039 platform, where eight I/O modules were installed. The input analog card (AI) NI-9229 is mainly used for control purposes, the analog output card (AIO) NI-9381 provides the current reference to the Keithley 2268 power supply, which controls the PM driver. The digital output card (DIO) NI-9401 is primarily used for relay control and for PWM signals. The analog output card provided the current reference to the dc power supply, which controls the dc motor driver.

IV. Model Validation

To provide a more comprehensive range of validation, this section shows the model validation of the positive sequence when the generator sweeps from sub-synchronous to hyper-synchronous operation under unbalanced grid conditions. The speed is controlled through a classic closed-loop speed control implemented in the dq-reference frame; details can be found in [8,24]. Validating the positive sequence is important because it contains information about the power exchange between the generator stator and the grid. A correct estimation of this sequence is required for a precise power flow analysis. To quantify the deviation between the measurements and the model estimated currents, this article uses the same criteria as in [20] where the following expression is used:

$$Error_{\%} = \left|\frac{I_{\,measured} - I_{\,model}}{I_{\,measured}}\right| 100 \le 10\% \tag{9}$$

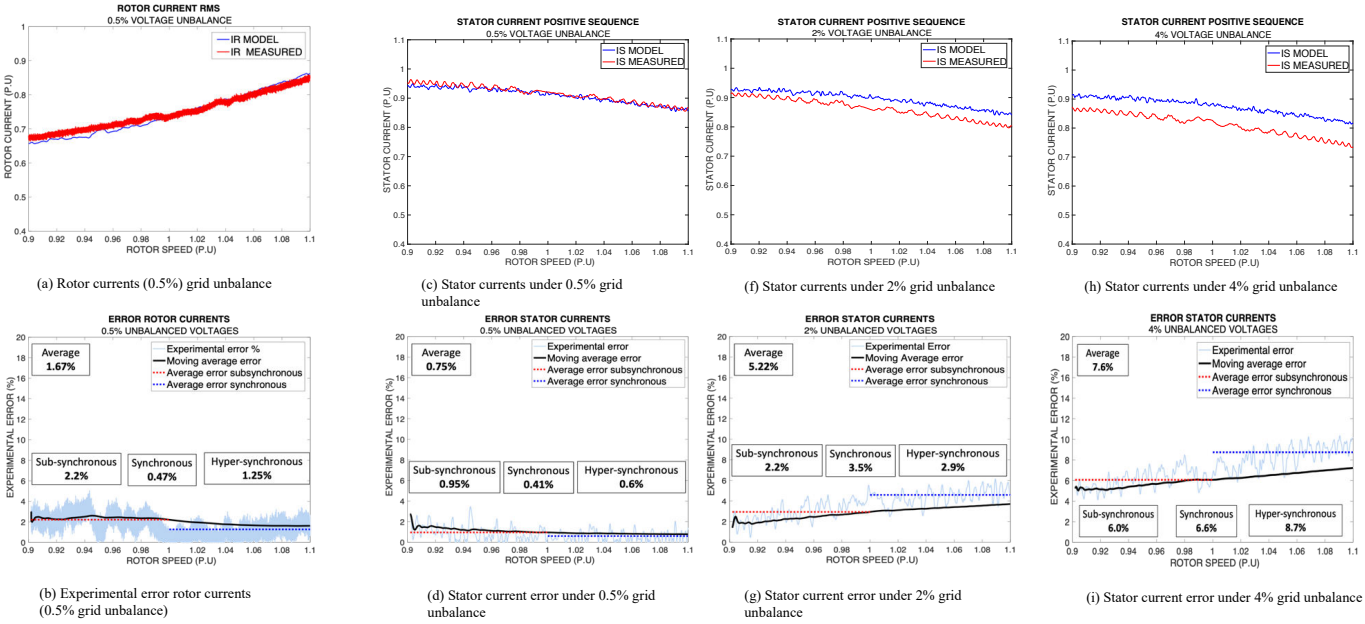

(a) Rotor currents (0.5%) grid unbalance

(c) Stator currents under 0.5% grid unbalance

(f) Stator currents under 2% grid unbalance

(h) Stator currents under 4% grid unbalance

(b) Experimental error rotor currents (0.5% grid unbalance)

(d) Stator current error under 0.5% grid unbalance

(g) Stator current error under 2% grid unbalance

(i) Stator current error under 4% grid unbalance

Figure 5: Positive Sequence Machine with iron losses for unbalanced grid conditions.

where I is either the stator or rotor current's positive sequence value in per unit. The model is declared valid if more than 85% of the samples do not exceed 10% of deviation allowed for a wide range of operation.

Fig. 5(a) shows the rotor and stator current results when the grid voltages have a 0.5%, 2% and 4% unbalance. Fig. 5(b) shows the estimation for the rotor currents is excellent, with an error between the model and measurement below 10% for all data points with an average error of 1.67%. This paper only presents the rotor currents for 0.5% grid voltage unbalance because for the other two cases [2%, 4%] the estimation was also very accurate.

Fig. 5 (c)-(i) show that the error of stator current positive sequence depends on the operation speed of the machine and the amount of unbalance. The higher the unbalance, the higher the deviation between the model and measurements. For 0.5% and 2% unbalance, all the datapoints remained under the 10% threshold with an average error of 0.75% and 5.22% respectively. Although the error is higher when the voltages are severely unbalanced (4%), 90.5% of the datapoints remained under the specified deviation with an average error of 7.6%. Therefore, we can conclude that the stator positive sequence and rotor currents are valid under a wide range of speeds and grid voltage unbalances. It is important to note that severe unbalances are not typical in grid tied DFIG as grid standards across the globe have specified the suitable limit for voltage unbalance for wind. These standards generally vary between 1% and 2% [23]. Fig. 5 results can be found in high resolution online in [24].

As seen in Fig. 6., the DFIG dynamic model can represent unbalanced currents, and as expected, the amount of unbalance is dependent on how severe the grid unbalance is. An inspection in *abc* coordinates shows that the estimated and measured unbalance current is similar for all tested grid unbalance. The discrepancy in the amount of unbalance may be the result of physical imbalances in the stator and rotor windings, which would result in different parametrization per phase. For reference, the models that are widely used in the literature such as $dq0$ and $\alpha\beta$ reference frames, as well as the model validated in this paper, assume perfectly balanced windings. It is worth pointing out that estimating the machine parameters per-phase is cumbersome. Methods such as the

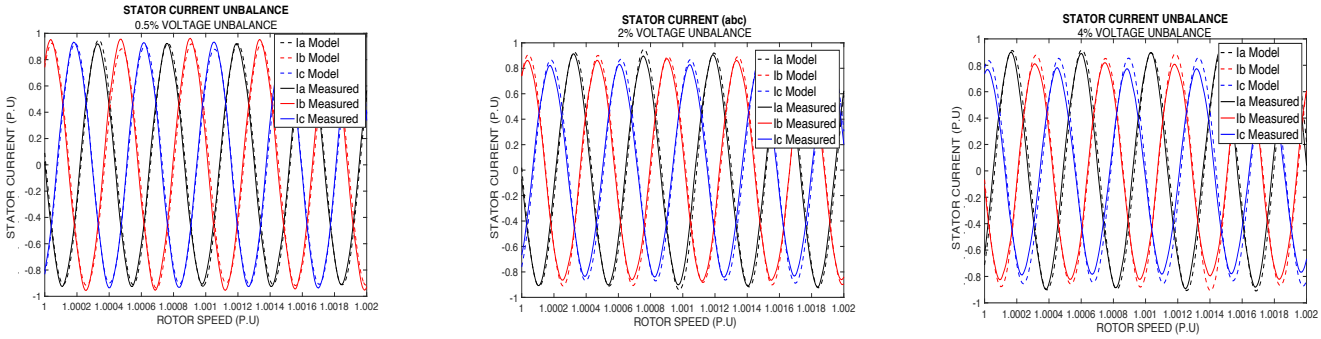

(a) (abc) stator currents under 0.5% grid unbalance

(b) (abc) stator currents under 2% grid unbalance

(c) (abc) stator currents under 4% grid unbalance

Figure 6: Validation of DFIG stator currents with iron losses for unbalanced grid conditions

locked rotor test, which is used to estimate the rotor and stator leakage inductances, assume a symmetrical machine per phase and do not allow an estimation these parameters separately. Furthermore, the estimation of the magnetizing inductance and the iron losses through the non-load test also assume a symmetrical machine.

V. Conclusions

This paper presented the development and the model validation of a real-time emulator of doubly fed induction generator (DFIG) wind turbine system. The code of the real-time DFIG dynamic model with iron losses, back-to-back model, mechanical model, and aerodynamic model were addressed in detail. The proposed discrete-modelling approach for real-time applications provides a flexible platform that can be utilized for analyzing and testing grid-connected DFIG systems. The discrete-time modeling and the implementation process results in a platform-independent model that is suitable for the application on any RT platform. The model validation was presented under different grid unbalances and for speeds ranging from the sub-synchronous to hyper-synchronous operation. These preliminary results showed that the DFIG model provides a good representation of the generator stator and rotor current positive sequence over a wide operating range and grid unbalances. This study represents an important initial step towards demonstrating the DFIG model's limitations in representing physical machinery under unbalanced grid conditions. Because most studies rely on these models to evaluate the reliability of an operating DFIG, validating this model is increasingly urgent and necessary due to the higher penetration of renewable energy technologies in the electric grid.

References

[1] Abad G, López J, Rodríguez MA, Marroyo L, Iwanski G. *Doubly Fed Induction Machine: Modeling and Control for Wind Energy Generation Applications*. Book, Chapters 1-15. Wiley-IEEE Press, 2011. Available: https://ieeexplore.ieee.org/book/6047757. Accessed: 2/12/21.

[2] "Global Wind Report 2021 | Global Wind Energy Council", *Global Wind Energy Council*, 2021. [Online]. Available: https://gwec.net/global-wind-report-2021/. [Accessed: 25- Jun- 2021]

[3] G. F. Gontijo et al., "Modeling, Control, and Experimental Verification of a DFIG With a Series-Grid-Side Converter With Voltage Sag, Unbalance, and Distortion Compensation Capabilities," in *IEEE Transactions on Industry Application*s, vol. 56, no. 1, pp. 584-600, Jan.-Feb. 2020, doi: 10.1109/TIA.2019.2946950.

[4] Federal Energy Regulatory Commission (FERC), United States of America. Docket no. RM05-4-000 Order no. 661. Interconnection for Wind Energy, pp. 1-85, Jun. 2, 2005. Available: https://www.ferc.gov/industries-data/electric/electric-transmission/generator-interconnection/standard-interconnection-0. Accessed: 2/12/21.

[5] M. Ferrari, "GSC control strategy for harmonic voltage elimination of grid-connected DFIG wind turbine," 2014 International Conference on Renewable Energy Research and Application (ICRERA), 2014, pp. 185-191, doi: 10.1109/ICRERA.2014.7016554.

[6] Wenzhong D, Muljadi E, Wang W. Comparison of Standards and Technical Requirements of Grid Connected Wind Power Plants in China and the United States. National Renewable Energy Laboratory of the U.S. Department of Energy, Report: NREL/TP-5D00-64225, September 2016. Available: https://doi.org/10.2172/1326717. Accessed: 2/12/21.

[7] Morfin OA, Ruiz-Cruz R, Loukianov AG et al.: Torque controller of a doubly-fed induction generator impelled by a DC motor for wind system applications. *IET Renew. Power Gener.,* 2014; 8(5):484-497. Available: https://doi.org/10.1049/iet-rpg.2012.0291 . Accessed: 2/12/21.

[8] Pena P, Clare JC, Asher GM. Doubly fed induction generator using back-to-back PWM converters and its application to variable-speed wind energy generation. IEE Proc., Electr. Power Appl., 1996; 143(3): 231–241. Available: https://doi.org/10.1049/ip-epa:19960288. Accessed: 2/12/21.

[9] H. Dehnavifard, M. A. Khan and P. S. Barendse, "Development of a 5-kW Scaled Prototype of a 2.5 MW Doubly-Fed Induction Generator," in *IEEE Transactions on Industry Applications,* vol. 52, no. 6, pp. 4688-4698, Nov.-Dec. 2016, doi: 10.1109/TIA.2016.2591512.

[10] M. E. Iranian, M. Mohseni, S. Aghili, A. Parizad, H. R. Baghaee and J. M. Guerrero, "Real-Time FPGA-based HIL Emulator of Power Electronics Controllers using NI PXI for DFIG Studies," in *IEEE Journal of Emerging and Selected Topics in Power Electronics*, doi: 10.1109/JESTPE.2020.3023100.

[11] L. Ibarra, A. Rosales, P. Ponce, A. Molina and R. Ayyanar, "Overview of Real-Time Simulation as a Supporting Effort to Smart-Grid Attainment", *Energies*, vol. 10, no. 6, p. 817, 2017.

[12] H. Shao et al., "Design and application of RTDS & GH Bladed co-simulation research platform for DFIG wind turbine," 8th Renewable Power Generation Conference (RPG 2019), 2019, pp. 1-8, doi: 10.1049/cp.2019.0366.

[13] Benigni A, Adler F, Fetzer D, Monti A, DeDoncker R. Real-time simulation of a doubly fed induction generator wind turbine on a new DSP based hardware platform. 15th European Conference on Power Electronics and Applications, Lille, France, 2013:1-10. Available: https://doi.org/10.1109/EPE.2013.6634687. Accessed: 2/12/21.

[14] Huerta F, Tello RL, Prodanovic M. Real-Time Power-Hardware-in-the-Loop Implementation of Variable-Speed Wind Turbines. *IEEE Transactions on Industrial Electronics,* 2017; 64(3):1893-1904. Available: https://doi.org/10.1109/TIE.2016.2624259. Accessed: 2/12/21.

[15] L. Pak and V. Dinavahi, "Real-Time Simulation of a Wind Energy System Based on the Doubly-Fed Induction Generator," in *IEEE Transactions on Power Systems*, vol. 24, no. 3, pp. 1301-1309, Aug. 2009, doi: 10.1109/TPWRS.2009.2021200.

[16] L. Trilla, O. Gomis-Bellmunt, A. Junyent-Ferre, M. Mata, J. Sanchez Navarro and A. Sudria-Andreu, "Modeling and Validation of DFIG 3-MW Wind Turbine Using Field Test Data of Balanced and Unbalanced Voltage Sags," in *IEEE Transactions on Sustainable Energy*, vol. 2, no. 4, pp. 509-519, Oct. 2011, doi: 10.1109/TSTE.2011.2155685.

[17] S. Auddy, R. K. Varma, and M. Dang, "Field Validation of a Doubly Fed Induction Generator (DFIG) Model," in *Proc. IEEE Electrical Power Conference,* pp. 484-489, Oct. 2007.

[18] A. Petersson, T. Thiringer, L. Harnefors and T. Petru, "Modeling and experimental verification of grid interaction of a DFIG wind turbine," in *IEEE Transactions on Energy Conversion*, vol. 20, no. 4, pp. 878-886, Dec. 2005, doi: 10.1109/TEC.2005.853750.

[19] Veltman A, Pulle DWJ, De Doncker RW. Fundamentals of Electric Drives. Power Systems, Book, Springer, pp. 1-357, 2007. Available: https://link.springer.com/book/10.1007/978-1-4020-5504-1. Accessed: 2/12/21.

[20] G. F. Gontijo et al., "Modeling, Control, and Experimental Verification of a DFIG With a Series-Grid-Side Converter With Voltage Sag, Unbalance, and Distortion Compensation Capabilities," in *IEEE Transactions on Industry Applications*, vol. 56, no. 1, pp. 584-600, Jan.-Feb. 2020, doi: 10.1109/TIA.2019.2946950.

[21] N. Karakasis, E. Tsioumas, N. Jabbour, A. M. Bazzi and C. Mademlis, "Optimal Efficiency Control in a Wind System With Doubly Fed Induction Generator," in IEEE Transactions on Power Electronics, vol. 34, no. 1, pp. 356-368, Jan. 2019, doi: 10.1109/TPEL.2018.2823481.

[22] Ferrari M, Buckner MA. Comparison of Doubly-Fed Induction Generator Machine Models for Real-Time Simulations. 9th IEEE International Symposium on Power Electronics for Distributed Generation Systems, Charlotte, NC, 2018, pp. 1-5. Available: https://doi.org/10.1109/PEDG.2018.8447730. Accessed: 2/12/21.

[23] W. E. Vanço, F. B. Silva and J. R. B. A. Monteiro, "A Study of the Impacts Caused by Unbalanced Voltage (2%) in Isolated Synchronous Generators," in *IEEE Access*, vol. 7, pp. 72956-72963, 2019, doi: 10.1109/ACCESS.2019.2919298.

[24] https://code.ornl.gov/f4e/labview-based-dfig-real-time-simulator.git